ARCHIVES
of
FOUNDRY ENGINEERING

ISSN (2299-2944)
Volume 2026
Issue 2/2026

212 – 222

10.24425/afe.2026.158009

26/2

Published quarterly as the organ of the Foundry Commission of the Polish Academy of Sciences

Effect of Bainitisation Temperature on Phase Transformation Kinetics in Silicon-Alloyed Cast Steels

R. Saraczyn [a, *], M. Deroszewska [a], S. Marciniak [b], D. Myszka [a]
[a] Faculty of Mechanical and Industrial Engineering, Warsaw University of Technology, Pl. Politechniki 1, 00-665 Warsaw, Poland
[b] Faculty of Materials Science and Engineering, Warsaw University of Technology, Pl. Politechniki 1, 00-665 Warsaw, Poland
* Corresponding author: E-mail address: robert.saraczyn.dokt@pw.edu.pl

Received 27.02.2026; accepted in revised form 31.03.2026; available online 14.07.2026

Abstract

This study investigates the effect of bainitisation temperature on the kinetics of phase transformation and the resulting microstructure in cast steels with two different silicon levels (0.87 wt.% and 2.06 wt.%). Cast steels were produced by induction melting and centrifugal casting. The remaining alloying elements were kept similar between alloys. A combined approach of JmatPRO simulations, high-resolution dilatometry, XRD, SEM, and Vickers hardness testing was used to characterise transformation temperatures, phase fractions, morphology and mechanical response. Results show that silicon exerts both thermodynamic and kinetic influences: thermodynamically, it tends to favour ferrite in equilibrium phase fields, while kinetically, it suppresses carbide precipitation during bainitic transformation, promoting carbon partitioning to austenite and thus increasing the fraction of retained austenite after austempering. Compared to the lower-Si alloy, the higher-Si alloy exhibits a bainitic transformation shifted to lower temperatures, higher hardness in fully transformed and quenched conditions, and larger retained-austenite fractions after isothermal bainitisation. Proper selection of bainitisation temperature in high-silicon cast steels enables favourable mechanical properties while retaining silicon-related benefits such as improved oxidation resistance and tempering stability.

Keywords: Silicon cast steel, Bainite, Austenite, Ferrite, Phase transformation

1. Introduction

With ongoing industrial development, the demand for materials with tailored mechanical and functional properties continues to grow. Such materials should combine high strength, thermal and chemical resistance with desirable magnetic, electrical, or optical properties, while maintaining low density. Their performance is governed by the relationship between chemical composition, microstructure, and processing, particularly solid-state transformations [1-6]. In metallurgy, researchers distinguish diffusion and non-diffusion transformations, such as austenitic and martensitic transformations. The bainitic transformation is an intermediate transformation upon cooling from austenite, the product of which is the bainite microstructure. Bainite has been characterised as a plate-like microstructure that is generally formed over a wide temperature range, typically between 125 °C and 550 °C [7]. In practice, the transformation commonly occurs when the steel is subcooled to temperatures between about 200 °C and 450

°C, combining diffusionless ferrite formation with subsequent diffusive carbon redistribution. As a result of the transformation, bainite, which is a mixture of ferrite saturated with carbon and dispersed carbides, is formed. Bainite nucleation begins the diffusive movement of carbon in austenite to grain boundaries and dislocations. The transformation nuclei are carbon-depleted regions formed near grain boundaries and dislocations. In the case of bainite, it can be expected very high hardness values, where the microstructure (600–700 HV) almost matches that of the hardest untempered martensite. It is worth noting that bainitic microstructures formed at exceptionally low transformation temperatures exhibit an unprecedented combination of high strength, hardness, and toughness [8].

The isothermal bainitic transformation is based on the decomposition of austenite into bainitic ferrite and carbides. During this process, only interstitial atoms, mainly carbon, can diffuse. This means that the formation and growth of carbides are determined by carbon migration. The precipitation of carbides can be controlled by adding the appropriate amount of silicon from the point of view of the thermodynamic stability of the carbide-silicon system. When steel has a sufficient silicon content, carbon cannot form carbides during the bainitic reaction. Instead, it diffuses into the surrounding austenite that encases the growth of bainite laths. As transformation progresses, the austenite continues to absorb carbon until a metastable equilibrium is reached between the bainitic ferrite and the carbon-enriched austenite. At this stage, the bainitic transformation halts, leaving some austenite untransformed [9]. Therefore, if silicon content is below the critical value during the bainitic reaction, carbon is more likely to form carbides within the bainitic structure rather than diffusing into the surrounding austenite. This carbide precipitation within bainite decreases the carbon available to enrich the austenite, which can hinder the formation of a carbon-enriched austenite phase and disrupt the intended metastable equilibrium.

Bainite is typically formed through an isothermal heat treatment performed above the martensite start temperature (Ms). Previous studies indicate that silicon contents above approximately 1.5 wt.% are generally required to suppress carbide precipitation during bainitic transformation, thereby promoting the formation of carbide-free bainite. Under these conditions, the final microstructure consists of a refined arrangement of bainitic ferrite plates interwoven with thin films of carbon-enriched retained austenite [10].

Silicon is used in the steel production process as a deoxidiser. Its chemical content increases the strength and hardness in the annealed state. Silicon steel containing about 3 wt.% Si is broadly used as a core material of transformers because of its good magnetic permeability and low core loss along the rolling direction [11]. Studies show that the presence of silicon promotes the growth of ferrite, which has a beneficial effect on alloy strength while decreasing its ductility [12, 13]. In recent years, research on carbide-free bainitic steels has primarily focused on steels that were previously homogenised and hot rolled, meaning they were thermomechanically treated to reduce solute segregation and refine their solidification structures [14]. Research shows that the higher silicon wt.% changes the microstructure from single-phase dominated to a more duplex structure with ferrite and austenite present. While moderate Si levels (~ 2-6 wt.%) improve strength and ductility, higher levels (~6 wt.%) transform the microstructure further, significantly reducing ductility and toughness [15]. Therefore, understanding the influence of silicon content and heat treatment parameters on bainitic transformation kinetics is essential for designing cast steels with controlled properties.

Heat treatment of iron alloys modifies their microstructure, resulting in changes in mechanical properties. Processes such as normalising, hardening, and tempering alter these properties, with hardening increasing strength, while normalising and tempering optimise the balance between strength and toughness. Hardness, depending on the specific nature of the transformation, usually develops in the austempering and hardening processes. For ductile iron and malleable iron, toughness increases in the austempering process. It has been observed that the normalising process refines grain size and enhances mechanical properties by transforming the microstructure to a more uniform state [16, 17]. In the austempering process for Austempered Ductile Iron (ADI), a bainitic structure – commonly referred to in the literature as ausferrite – is formed, which is characterised by very good mechanical properties, combining high strength, toughness, and wear resistance [18, 19].

Silicon plays a critical role in steels by strongly influencing phase transformation kinetics and the stability of microstructural constituents, with its function differing between low- and medium-carbon steels. While high-silicon, low-carbon steels are commonly employed in electromagnetic applications due to their favourable magnetic properties, in medium-carbon cast steels this effect is primarily associated with phase transformation kinetics. In contrast to electrical steels, medium-carbon silicon-alloyed cast steels are primarily developed for structural and wear-resistant applications, such as gears, shafts, and components operating under high mechanical loads, where a combination of high strength, hardness, and adequate toughness is required. In these alloys, silicon promotes the formation of bainitic microstructures by suppressing carbide precipitation and enabling carbon partitioning to retained austenite. As a result, high-silicon medium-carbon cast steels offer a promising alternative to conventional heat-treated cast steels and ADI in demanding mechanical applications.

However, increased silicon content may reduce ductility, necessitating careful control of heat treatment and microstructure. Despite extensive research on bainitic steels, its influence on solid-state transformations in medium-carbon cast steels remains insufficiently understood, particularly in terms of kinetics and resulting microstructures. This study therefore investigates these effects through controlled variation of composition and heat treatment to optimise the balance between hardness and resistance to brittle fracture.

2. Methodology

In this work, the influence of different silicon levels and process temperatures in two cast steels on the kinetics of the bainite transformation is being examined. For this purpose, a series of tests has been conducted on the previously prepared alloys with different silicon content and similar content of other elements. During the research following methods have been used: scanning electron microscopy (SEM), computer dilatometry simulations, physical dilatometry tests, X-ray diffraction analysis and microhardness tests.

2.1. Materials

Cast steel has been produced by melting in a medium-frequency induction furnace with a crucible capacity of 240 mm on a BEGO Fornax 35K device.

Centrifugal casting was made in a graphite mould with the shape of a recess in the form of a pellet with dimensions of ø50x12mm.

The chemical composition of the two types of cast steel is presented in Table 1.

Table 1.
Chemical composition (wt.%) of analysed alloys

Material	C	Si	Mn	P	S	Cu	Cr	Mo	Ni	W	Al	Co	Fe
Cast Steel 1	0.70	0.87	0.19	0.007	0.006	0.06	0.57	0.31	1.44	0.36	0.01	0.01	bal.
Cast Steel 2	0.67	2.06	0.21	0.017	0.003	0.07	0.63	0.38	1.46	0.23	0.01	0.01	bal.

The materials for testing, in two variants, were selected in such a way that the content of chemical elements other than silicon did not affect the process of transformations in the solid state. Moreover, for Cast Steel 1 (CS1), the silicon content was below the critical value of 1.5 wt.% indicated in the literature [14] and for Cast Steel 2 (CS2), above this value.

2.2. Research instrumentation

On the basis of the chemical compositions, presented in Table 1, thermodynamic and kinetic simulations were performed using JMatPro to generate TTT and CCT diagrams for austenitisation temperatures in the range of 750–1150 °C. The software enables simulation of phase transformations and prediction of material properties based on input composition [20, 21]. In this study, it was used to determine the optimal austenitisation temperature and to predict the expected dilatometric behaviour. Based on these simulations, 900 °C was selected as the optimal austenitisation temperature, as further increases did not result in a significant decrease in martensite start temperature (Ms) or a substantial extension of bainitic incubation time.

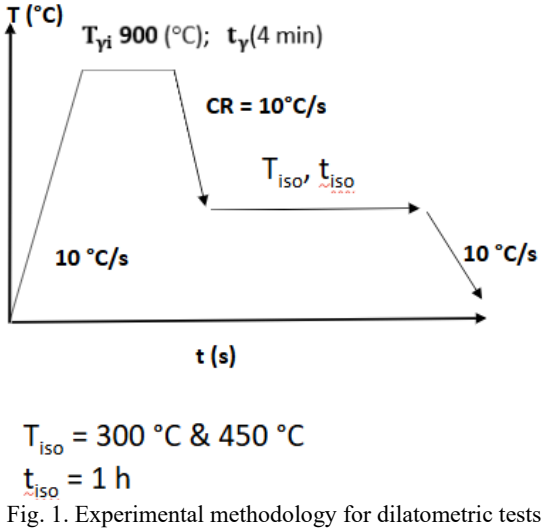

Fig. 1. Experimental methodology for dilatometric tests

A dilatometer is a laboratory instrument used to measure dimensional changes in a material as a function of temperature, enabling the analysis of thermal expansion and phase transformations during heating and cooling. It allows to measure the linear thermal expansion of solids. When examining new metal alloys and their properties, dilatometry is used for research on solid-state transformation parameters [22, 23]. A dilatometer used in the test was a high-resolution Bahr 805A, which is fully controlled by the computer. The temperature of the specimen was continuously monitored using a K-type thermocouple spot-welded to the mid-length of the sample's surface. Fused silica push rods, which have a thermal expansion coefficient of 0.54×10^{-6} °C^{-1}, were in contact with the samples. A linear variable differential transducer (LVDT) was employed to measure the changes in sample length. In the study values such as temperature and change in length as a function of time are obtained, which allows the creation of graphs showing Continuous Cooling Transformation (CCT) and Time-Temperature Transformation (TTT). The process flow is shown in Figure 1. Transformation temperatures were determined using the tangent method, based on the intersection of linear fits to the dilatometric curves.

A Leitz Wetzlar hardness tester was used to measure the hardness of the samples. The test was carried out using the Vickers method with a load of 100g, according to DIN EN ISO 6507-1, to enable local characterisation of the heterogeneous microstructure.

XRD measurements were carried out with a Bruker AXS D8 diffractometer equipped with a Co X-ray tube, Goebel mirror optics and a LynxEye Linear Position Sensitive Detector. XRD measurements were performed with tube settings of 40 kV and 30 mA, in the coupled θ-2θ mode, spanning an angular range from 35° to 135°. The data were collected with a step size of 0.015° and a counting time of 2 seconds per step.

A Scanning Electron Microscope (SEM) was used to examine the microstructure, including plate thickness and arrangement of the phases. The research was carried out on a Hitachi SU8000. Secondary electron imaging was performed at 10 kV. Specimens were prepared following the standard metallographic procedures, including grinding and polishing.

3. Results and discussion

The results were analysed primarily with an emphasis on understanding the changes occurring during the bainitisation process. Dilatometric tests were performed using an austenitisation temperature of 900 °C, selected based on prior JMatPro simulations. Physical dilatometric tests were subsequently performed at this temperature.

Figures 2 and 3 show that under continuous cooling conditions, for a cooling rate of 0.1 °C/s, the formation of pearlite or ferrite and bainite is expected, whereas at higher cooling rates (1 °C/s, 10 °C/s, 100 °C/s) martensite formation predominates. However, these diagrams correspond to continuous cooling without isothermal holding, while some of the present experiments include an isothermal bainitisation step. The Ms temperature predicted by the software is 214 °C and 196 °C for CS1 and CS2, respectively. While compared to Figures 6a and 6b, the expected Ms temperatures are quite close to the actual values (204 °C and 206 °C). A comparison of Figures 4 and 5 indicates that the higher silicon content in CS2 results in the bainitic transformation occurring at temperatures approximately 30 °C lower than those observed for CS1.

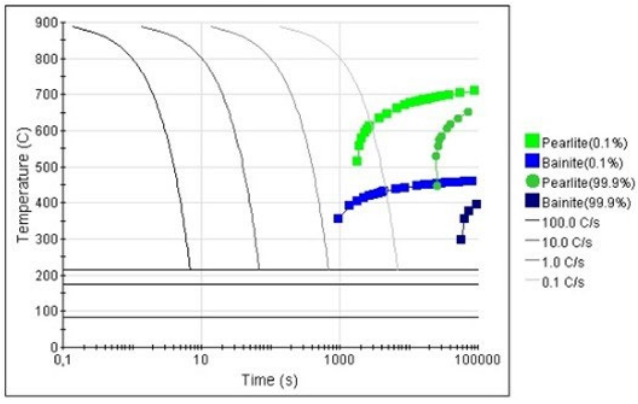

Fig. 2. CCT graph from JmatPRO software for Cast Steel 1

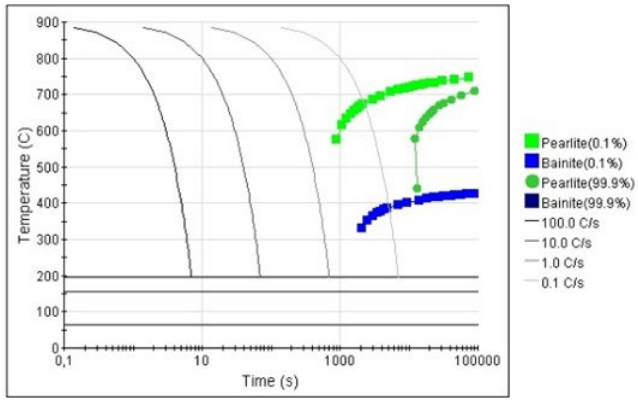

Fig. 3. CCT graph from JmatPRO software for Cast Steel 2

Figures 6a and 6b indicate no intermediate transformations occur for the analysed samples at the given process parameters. The formation of an austenitic structure is visible from the Ac1 temperature to the Ac3 temperature, and then martensite starts forming at the Ms temperature. The deviation observed at approximately 400–500 °C during heating is attributed to recovery processes and carbide evolution within the as-cast pearlitic microstructure, rather than to a phase transformation. In Figures 7a and 7b, martensitic transformation is not observed during cooling due to the combined effects of austenite consumption and stabilisation during bainitic transformation. For CS1-B-300, the bainitic reaction largely exhausts the available austenite, leaving insufficient material for martensitic transformation. For CS2-B-300, the higher silicon content enhances carbon enrichment and stabilises the remaining austenite, suppressing martensite formation. Additionally, internal stresses generated during bainite formation impose mechanical constraints that further inhibit martensitic transformation. Both austempered samples (Figures 8a and 8b) exhibit martensite formation upon cooling. In CS1-B-450 (Figure 8a), martensitic transformation initiates at approximately 122 °C and is limited in extent, indicating that only a small fraction of austenite remains after the bainitic transformation. In contrast, CS2-B-450 (Figure 8b) shows a more pronounced martensitic transformation beginning at about 187 °C, suggesting the presence of a larger amount of metastable austenite. Therefore, following the austenitisation and bainitisation processes, a portion of the austenite remains insufficiently enriched in carbon to be fully stabilised, leading to its transformation into martensite during cooling. This is also reflected in Figures 9 and 10, where the relative change in sample length parameter indicates that the bainitisation process differed from that for the material with the lower silicon content. This observation is confirmed by the results of hardness tests presented in Table 3, since martensite is a hard phase [24, 25]. The hardness value for all CS2 samples is higher than that for the corresponding CS1. Compared to CS1-B-450, CS2-B-450 has 21% greater hardness. For CS2-10 and CS2-B-300 and their counterparts, it is 9% and 2%, respectively.

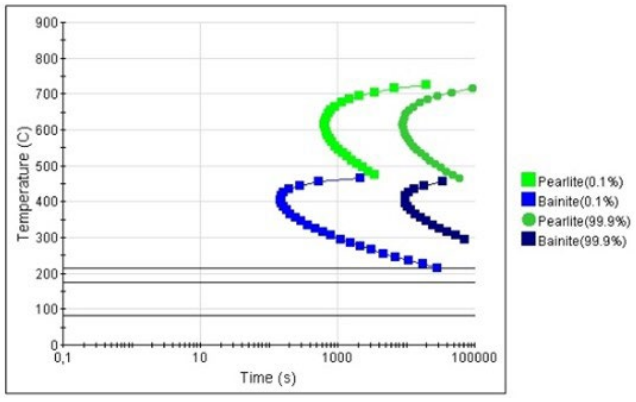

Fig. 4. TTT graph from JmatPRO software for Cast Steel 1

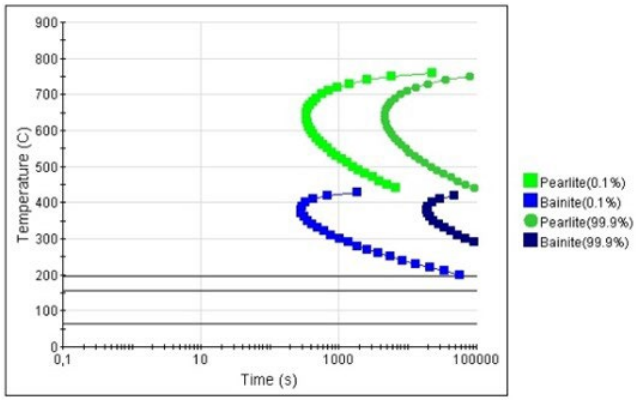

Fig. 5. TTT graph from JmatPRO software for Cast Steel 2

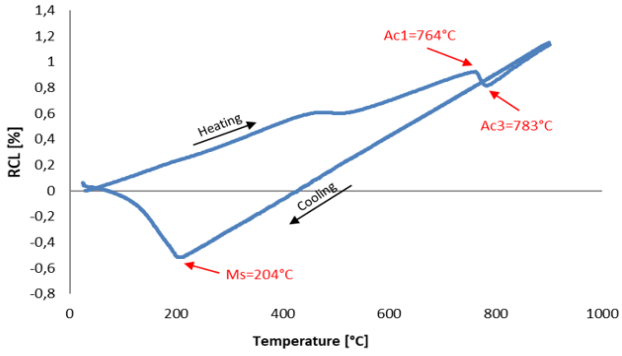

Fig. 6a. Dilatometric curve - heating to 900 °C with 10 °C/s rate, austenitisation at 900 °C and cooling with 10 °C/s rate – CS1-10

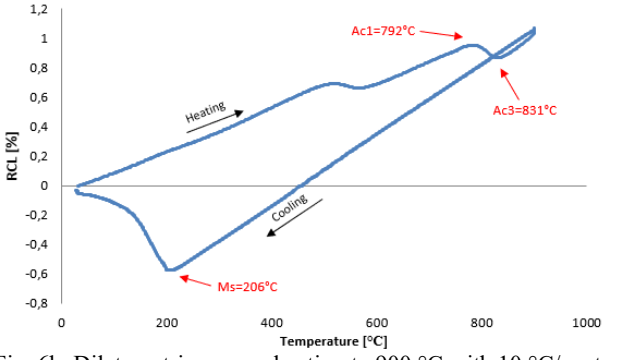

Fig. 6b. Dilatometric curve - heating to 900 °C with 10 °C/s rate, austenitisation at 900 °C and cooling with 10 °C/s rate – CS2-10

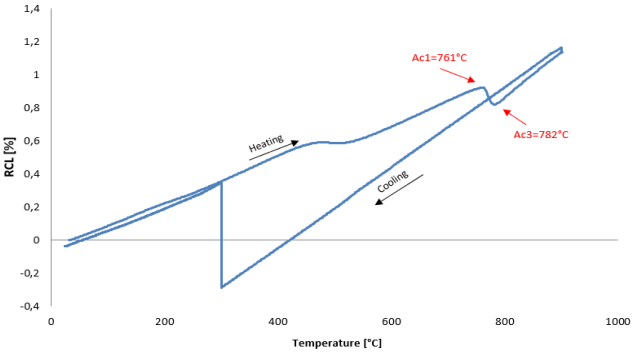

Fig. 7a. Dilatometric curve - heating to 900 °C with 10 °C/s rate, austenitisation at 900 °C, cooling to 300 °C, bainitisation at 300 °C and cooling with 10 °C /s rate – CS1-B-300

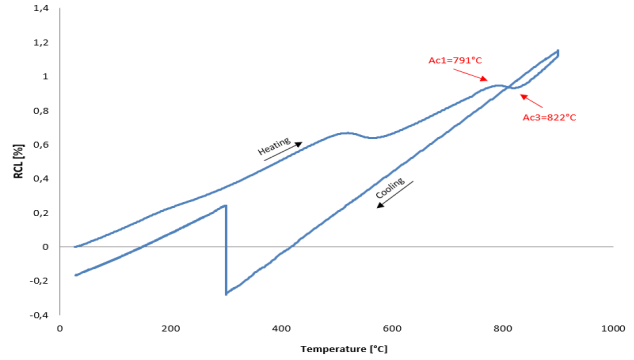

Fig. 7b. Dilatometric curve - heating to 900 °C with 10 °C/s rate, austenitisation at 900 °C, cooling to 300 °C, bainitisation at 300 °C and cooling with 10 °C /s rate – CS2-B-300

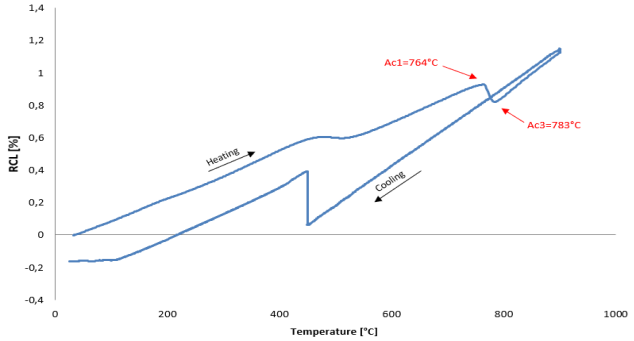

Fig. 8a. Dilatometric curve - heating to 900 °C with 10 °C/s rate, austenitisation at 900 °C, cooling to 450 °C, bainitisation at 450 °C and cooling with 10 °C/s rate – CS1-B-450

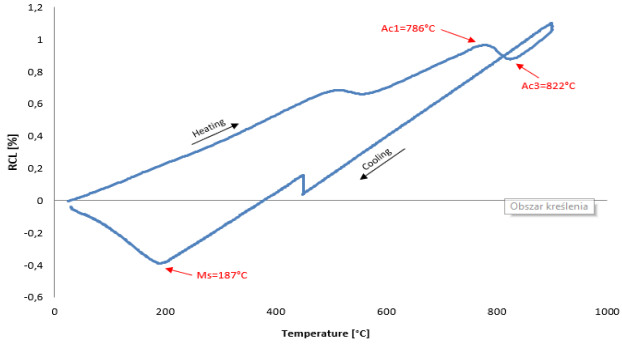

Fig. 8b. Dilatometric curve - heating to 900 °C with 10 °C/s rate, austenitisation at 900 °C, cooling to 450 °C, bainitisation at 450 °C and cooling with 10 °C/s rate – CS2-B-450

Table 2.
Characteristic temperatures – Ac1, Ac3, Ms

Sample	Bainitisation temperature [°C]	Ac1 [°C]	Ac3 [°C]	Ms [°C]
CS1-10	-	764	783	204
CS1-B-300	300	761	782	-
CS1-B-450	450	764	783	122
CS2-10	-	792	831	206
CS2-B-300	300	791	822	-
CS2-B-450	450	786	822	187

The results presented in Table 2 indicate that higher temperatures of Ac1 (start temperature for the transformation from pearlite into austenite) and Ac3 (finish temperature for the transformation from ferrite to austenite) are observed for higher %wt. of silicon. Since silicon influences the diffusion rates of carbon and other atoms within the iron matrix, slower diffusion rates will lead to higher transformation temperatures because of the longer time of redistribution of carbon, which is necessary for phase transformation. Moreover, the addition of silicon modifies the iron-carbon phase diagram. Silicon can expand the phase fields and shift the temperature ranges at which these transformations occur. Specifically, silicon tends to stabilise ferrite and can increase the eutectoid temperature, altering the temperatures at which transformations like pearlite or bainite formation start [26, 27].

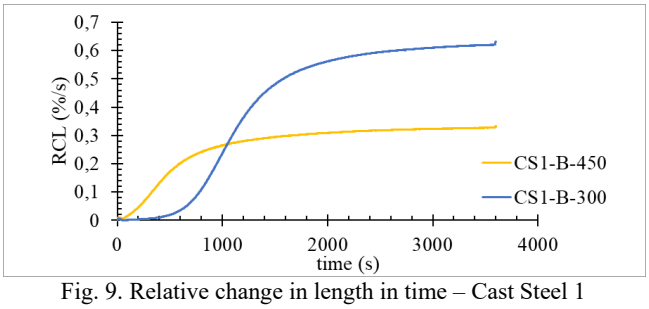

Fig. 9. Relative change in length in time – Cast Steel 1

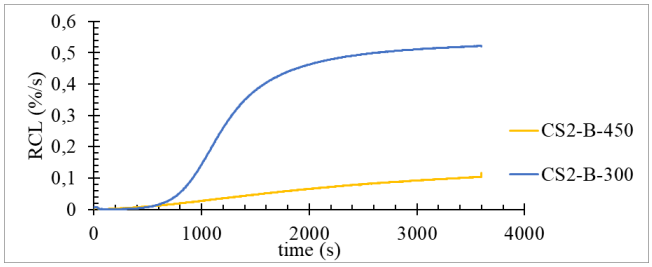

Fig. 10. Relative change in length in time – Cast Steel 2

Analysing Figures 9 and 10, the dilatometry results are consistent with bainitic transformation theory - the lower the temperature, the greater the relative length change [28]. Bainite forms in different morphologies depending on transformation temperature. At higher temperatures, the dilatometric change is smaller because a reduced fraction of austenite transforms within the given time, resulting in lower volumetric strain. In contrast, lower temperature bainite involves greater structural rearrangement and density difference, leading to larger volumetric changes. The nearly linear character of the CS2-B-450 curve indicates that the transformation proceeds only to a limited extent, which is consistent with the presence of martensite observed during subsequent cooling. In addition, carbide precipitation at higher temperatures may influence the dilatometric response; however, this effect is limited by silicon. It is worth noting that for bainitisation at 450 °C, both samples (CS1-B-450 and CS2-B-450) exhibit very short or indistinct incubation times. In contrast, both CS1-B-300 and CS2-B-300 show a measurable incubation period, with CS1-B-300 exhibiting the longest delay before transformation begins. This behaviour represents a deviation from the simulation

results, which predict similar incubation times for all investigated transformation conditions.

Figures 9, and 10 indicate that the transformations at lower temperatures occur similarly, but the higher the temperature of this transformation, the kinetics of the transformation begin to differ, and the processes occur more slowly, and up to a certain point. This indicates that silicon suppresses carbide precipitation processes.

Table 3.
Hardness test results

Sample	Average Hardness [HV]
CS1-10	674.3 (± 3.7%)
CS1-B-300	437 (± 3.9%)
CS1-B-450	263.7 (± 4.7%)
CS2-10	735.3 (± 2.5%)
CS2-B-300	445.7 (± 5.0%)
CS2-B-450	319 (± 5.0%)

Table 3 and Figure 11 indicate that the CS2 material exhibits higher hardness than CS1. This difference can be attributed to the higher silicon content in CS2, which enhances solid solution strengthening and, in samples containing martensite, leads to greater silicon supersaturation of martensite [29]. In addition, silicon is known to retard dislocation rearrangement and recovery processes in martensitic and bainitic structures, thereby contributing to increased hardness [30]. In the case of bainitisation at 300 °C, the hardness test results for both alloys are very similar since there was no transformation of austenite into martensite.

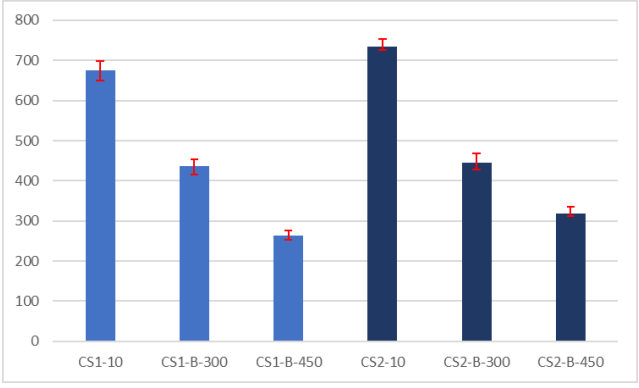

Fig. 11. Hardness test results

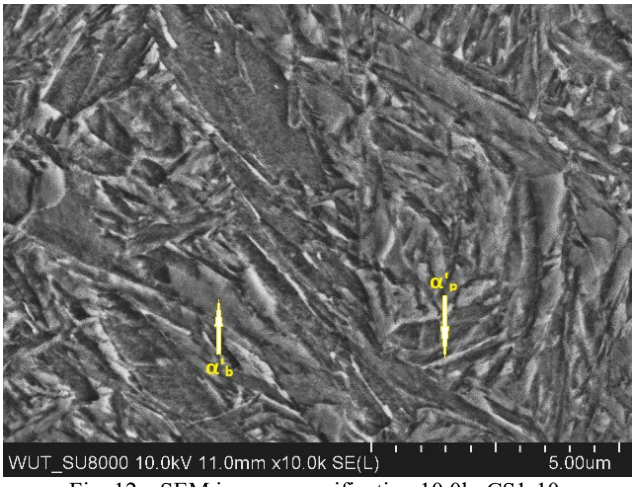

Fig. 12a. SEM image magnification 10.0k; CS1-10; α'_b – martensite block, α'_p – martensite plate

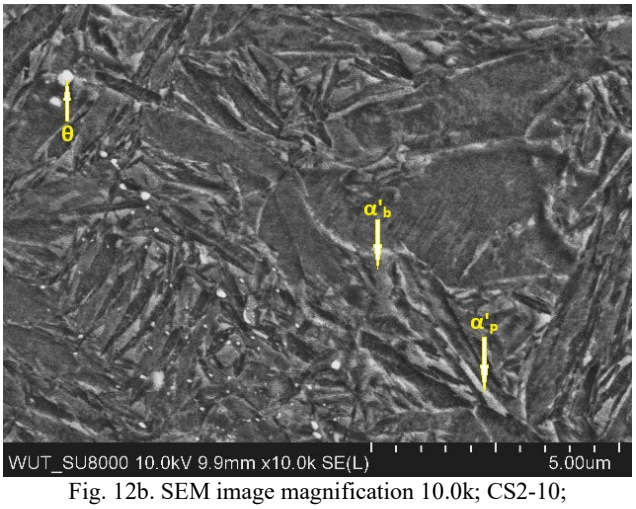

Fig. 12b. SEM image magnification 10.0k; CS2-10; α'_b – martensite block, α'_p – martensite plate, θ – carbide

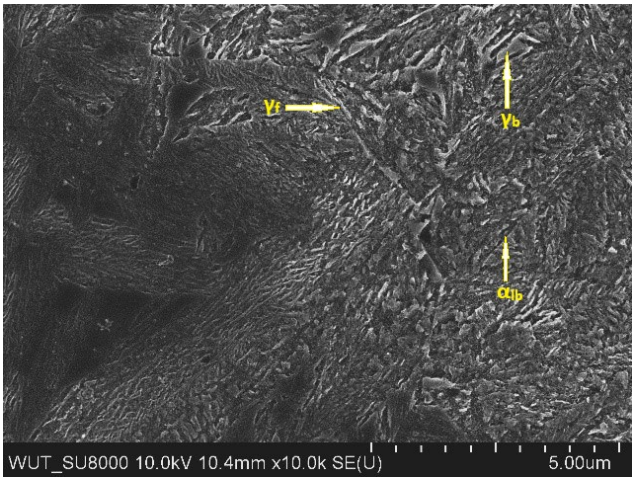

Fig. 13a. SEM image magnification 10.0k; CS1-B-300; γ_f – austenite film, γ_b – austenite block, α_{lb} – bainitic ferrite

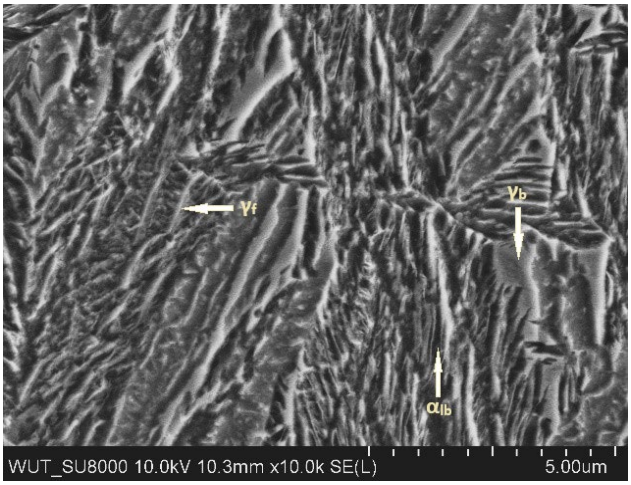

Fig. 13b. SEM image magnification 10.0k; CS2-B-300; γ_f – austenite film, γ_b – austenite block, α_{lb} – bainitic ferrite

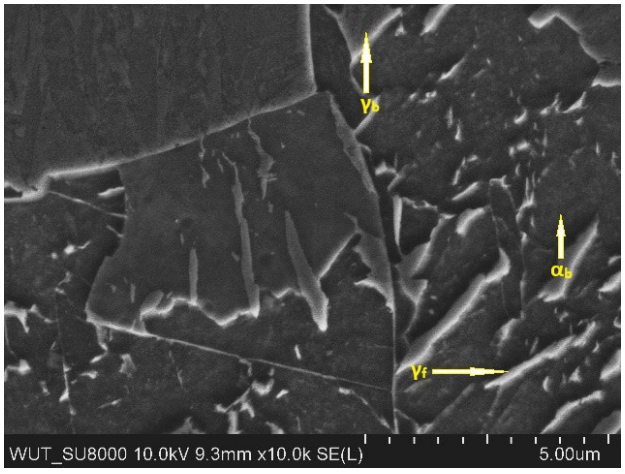

Fig. 14a. SEM image magnification 10.0k; CS1-B-450; γ_f – austenite film, γ_b – austenite block, α_b – bainitic ferrite

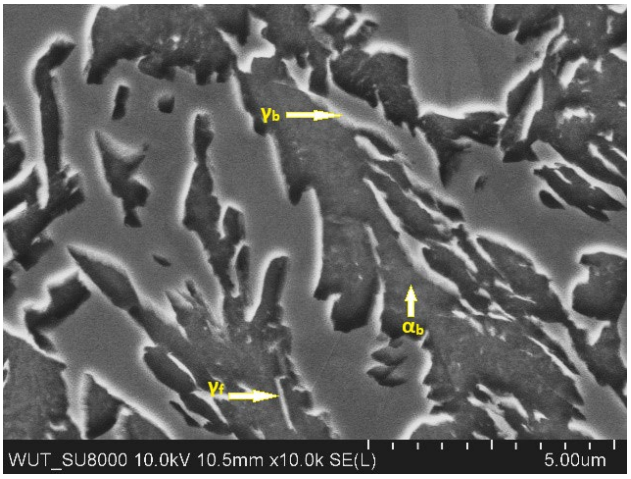

Fig. 14b. SEM image magnification 10.0k; CS2-B-450; γ_f – austenite film, γ_b – austenite block, α_b – bainitic ferrite

Figure 12 shows two samples subjected to the austenitisation process and then cooled to room temperature without any intermediate processes. The structure observed in both cases is comparable, where martensite with a similar morphology is formed. It is a mix of plate-like and lath-like martensite, where thick plates are dominant. This is consistent with previous studies on the mechanisms of martensite formation at different carbon contents, where for steels up to 0.6 wt.% C the microstructure will be lath-like, above 1 wt.% C plate-like, and in between it will be a mix of both [31-33]. Clusters of carbides are visible in Figure 12b. For the CS2-10 sample, these features are attributed to incomplete dissolution of carbides during austenitisation, as well as possible formation of fine transition carbides associated with auto-tempering of martensite. While silicon suppresses cementite precipitation, it does not fully inhibit the formation of transition carbides in a highly supersaturated martensitic structure.

Microstructures observed after the bainitisation process (Figures 13 and 14) differ based on the temperature and silicon content. Figure 13 presents a plate-like microstructure, which is typical for lower bainite [34, 35]. Figure 14 shows an island-like microstructure where bainitic ferrite blocky islands are separated by carbon-rich austenite [36, 37]. The difference in morphology is related to the fact that lower bainite cooler transformation temperatures restrict carbon diffusion. Slower diffusion causes carbon to remain longer within the supersaturated bainitic ferrite, forming fine carbide particles inside the ferrite plates, creating a plate-like microstructure with dispersed internal carbides [35]. However, upper bainite forms at higher transformation temperatures, allowing carbon to diffuse more easily. Consequently, carbon exits the bainitic ferrite faster and precipitates as carbides at the boundaries between the ferrite and the surrounding austenite. This results in an island-like microstructure, with minimal internal carbide precipitation within the ferrite [37].

Differences in morphology can be noticed by comparing Figure 13a to 13b and Figure 14a to 14b. Despite the same bainitisation temperatures, the microstructures are slightly different. The plates (Figure 13b) and islands (Figure 14b) for the CS2 alloy are more homogeneous than those of CS1, with a more orderly arrangement and parallelism to each other. With silicon suppressing carbide formation, the bainitic ferrite tends to form without significant internal carbide precipitation. This results in a cleaner bainitic structure, with finer and more homogeneous arrangement [38, 39].

The microstructural analysis allows an understanding of the relationship between phase morphology and hardness (Figure 11). The presence of fine carbide precipitates within the plates of bainitic ferrite is a key factor in the higher hardness of lower bainite compared to upper bainite. In the case of upper bainite, carbon tends to diffuse out of the bainitic ferrite more easily, leading to carbide formation at the boundaries of the ferrite islands rather than inside them. This results in a softer overall structure for upper bainite [40].

Table 4.
XRD analysis results – percentage content of austenite and bainitic-ferrite phases

Sample	Austenite [%]	Ferrite [%]
CS1-B-300	11.73	88.27
CS1-B-450	11.37	88.63
CS2-B-300	21.64	78.36
CS2-B-450	19.34	80.66

The results of the diffraction analysis shown in Table 4 indicate that a higher silicon content in the material results in a higher content of the austenite phase in the solid state after the heat treatment process. Silicon also affects phase stability in steels by strongly suppressing carbide precipitation during heat treatment. As a result, carbon is prevented from forming cementite and instead partitions into the austenite. Consequently, a higher fraction of retained austenite is preserved after heat treatment.

Samples CS1-B-300 and CS1-B-450 are characterised by similar phase composition, with a slightly higher austenite share for the sample bainitized at 300 °C. In the case of CS2-B-300 and CS2-B-450, this difference is more significant. At higher transformation temperatures enhanced carbon partitioning prevents austenite from transforming into bainite or martensite, which observation corresponds with Figures 13 and 14.

4. Conclusions

The increase in the silicon content in cast steels is affecting the solid-state transformations by altering the basic characteristics of steel, including its transformation temperatures. The addition of silicon modifies the iron-carbon phase diagram. Silicon can expand the phase fields or shift the temperature ranges at which these transformations occur. Specifically, silicon tends to stabilise ferrite and can increase the eutectoid temperature.

Changing silicon content in cast steels fundamentally affects the internal structural dynamics of the material, leading to changes in the temperatures at which solid state transformations occur and therefore determining the material's properties, such as hardness.

Higher bainitisation temperatures are associated with shorter incubation times but reduced overall transformation strain, resulting in smaller relative length changes. In samples with higher silicon content, bainitic transformation is further limited due to enhanced carbon enrichment of austenite, leading to improved dimensional stability.

The hardness of cast steel is affected by silicon content due to its influence on solid-state transformations. By suppressing carbide precipitation and increasing carbon activity, silicon promotes carbon retention in solid solution and carbon enrichment of austenite, thereby modifying the bainitic and martensitic transformation behaviour and the resulting microstructure.

Despite similar Ms temperatures, increased silicon content enhances martensite hardness through solid solution strengthening and suppression of recovery processes, rather than by altering the martensitic transformation temperature.

The conducted studies have shown that silicon is an important element influencing solid-state transitions for silicon cast steels. Further research must focus on understanding the kinetics of these transitions depending on the different silicon content. This will allow the development of effective heat treatment processes for silicon cast steel and thus may increase the importance of these materials for industrial applications.

Acknowledgements

The dilatometry and XRD studies were carried out in cooperation with the Phase Transformation Laboratory and X-Ray Diffraction Laboratory of the National Center for Metallurgical Research (CENIM) in Madrid.

References

[1] Shin, J.-C., Lee, S. & Ryu, J.H. (1999). Correlation of microstructure and fatigue properties of two high-strength spring steels. *International Journal of Fatigue*. 21(6), 571-579. DOI: 10.1016/S0142-1123(99)00010-9.

[2] Qiu, J.-J., Zhang, M., Gao, G.-h., Tan, Z.-l. & Bai, B.-z. (2020). Research and modeling on correlation among microstructure, yield strength and process of bainite/martensite steel. *Journal of Iron and Steel Research International*. 27(7), 834-841. DOI: 10.1007/s42243-020-00389-x.

[3] Dixit, M., Mishra, R.S. & Sankaran. K.K. (2008). Structure–property correlations in Al 7050 and Al 7055 high-strength aluminum alloys. *Materials Science and Engineering: A*. 478(1-2), 163-172. DOI: 10.1016/j.msea.2007.05.116.

[4] Basu, S., Patra, A., Jaya, B.N., Ganguly, S., Dutta, M. & Samajdar, I. (2022). Study of microstructure-property correlations in dual phase steels for achieving enhanced strength and reduced strain partitioning. *Materialia*. 25(85005). DOI: 10.1016/j.mtla.2022.101522.

[5] Hamada, A.S., Jaskari, M., Ali, M., Kaijalainen, A. & Järvenpää, A. (2023). Impact of ultra-flash tempering treatment on the microstructure and mechanical properties of high-strength carbon steel. *Materials Science Forum*. 1105, 53-59. DOI: 10.4028/p-sP4Ffb.

[6] Delic, A., Oruču, M., Rimac, M., Gigović-Gekić, A. & Sunulahpašić, R. (2019). The influence of solution annealing on microstructure and mechanical properties heat-resistant cast Steel HK30 modified by Niobium. *Metallurgical and Materials Engineering*. 25(3), 237-245. DOI: 10.30544/430.

[7] Bhadeshia, H.K.D.H. (2013). The first bulk nanostructured metal. *Science and Technology of Advanced Materials*. 14(1), 014202, 1-7. DOI: 10.1088/1468-6996/14/1/014202.

[8] Bhadeshia, H. K. D. H. (2005). Hard bainite. In J. M. Howe, D. E. Laughlin, J. K. Lee, U. Dahmen, & W. A. Soffa (Eds.), *Solid–Solid Phase Transformations in Inorganic Materials* (Vol. 1, pp. 469–484). TMS.

[9] Kotesovec, V., Vorel, I., Jenicek, S., Kana, J., Ibrahim, K. (2017). Impact of quenching temperature and isothermal holding time during austempering on bainite content in high-silicon steel. In IOP Conference Series Materials Science and Engineering (Vol. 179, pp. 012041). DOI: 10.1088/1757-899X/179/1/012041.

[10] Santacruz-Londono, A.F., Rios-Diez, O., Jimenez, J.A., Garcia-Mateo, C. & Aristizabal-Sierra, R. (2020). Microstructural and mechanical characterization of a nanostructured bainitic cast steel. *Metals*. 10(5), 612, 1-14. DOI: 10.3390/met10050612.
[11] Wang, Y., Xu, Y.-B., Zhang, Y.-X., Fang, F., Lu, X., Liu, H.-T. & Wang, G.-D. (2015). Development of microstructure and texture in strip casting grain oriented silicon steel. *Journal of Magnetism and Magnetic Materials*. 379, 161-166. DOI: 10.1016/j.jmmm.2014.12.043.
[12] Stan, S., Riposan, I., Chisamera, M. & Stan. I. (2019). Solidification characteristics of silicon-alloyed ductile cast irons. *Journal of Materials Engineering and Performance*. 28, 278-286. DOI: 10.1007/s11665-018-3828-2.
[13] Alhussein, A., Risbet, M., Bastien, A., Chobaut, J.P., Balloy, D. & Favergeon, J. (2014). Influence of silicon and addition elements on the mechanical behaviour of ferritic ductile cast iron. *Materials Science and Engineering: A*. 605, 222-228. DOI: 10.1016/j.msea.2014.03.057.
[14] Basso, A., Toda-Caraballo, I., San-Martin, D. & Caballero, F.G. (2020). Influence of cast part size on macro- and microsegregation patterns in a high carbon high silicon steel. *Journal of Materials Research and Technology*. 9(3), 3013-3025. DOI: 10.1016/j.jmrt.2020.01.052.
[15] Setia, P., Venkateswaran, T., Tharian, K.T., Jain, J., Singh, S.S. & Shekhar. S. (2022). Influence of Si content on the microstructure and mechanical properties of silicon stainless steel. *Materials Science and Engineering: A*. 829, 14214. DOI: 10.1016/j.msea.2021.142141.
[16] Akinribide, O.J., Ogundare, O.D., Oluwafemi, O.M., Ebisike, K., Nageri, A.K., Akinwamide, S.O., Gamaoun, F. & Olubambi. P.A. (2022). A review on heat treatment of cast iron: phase evolution and mechanical characterization. *Materials*. 15(20), 7109, 1-38. DOI: 10.3390/ma15207109.
[17] Chang, S.K., Kim, D.G. & Choi. J.W. (1992). Effects of alloying elements and austenite destabilization heat treatment on graphitization of high chromium cast iron. *ISIJ International*. 32(11), 1163-1169. DOI: 10.2355/isijinternational.32.1163.
[18] Kang, Ch.-Y., Sung, J.-H., Kim, G.-Ho, Kim, B.-S. & Kim. I.-S. (2009). Effect of heat treatment on the damping capacity of austempered ductile cast iron. *Materials Transactions*. 50(6), 1390-1395. DOI: 10.2320/matertrans.MRA2008427.
[19] Boccardo, A.D., Dardati, P.M., Celentano, D.J., Godoy, L.A., Górny, M. & Tyrała, E. (2016). Numerical simulation of austempering heat treatment of a ductile cast iron. *Metallurgical and Materials Transactions B*. 47, 566-575. DOI: 10.1007/s11663-015-0511-y.
[20] Saunders, N., Guo, U.K.Z., Li, X., Miodownik, A.P. & Schille. J-Ph. (2003). Using *JMatPro* to model materials properties and behavior. *The Journal of The Minerals, Metals & Materials Society*. 55(12), 60-65. DOI: 10.1007/s11837-003-0013-2.
[21] Kang, G.P., & Lee, K.H. (2008). Calculation of material properties with JMatPro for the process simulation. In Proceedings of the 2008 Spring Conference of the Korean Society for Technology of Plasticity (pp. 142–145).
[22] Garcia de Andres, C., Caballero, F.G., Capdevila, C. & Alvarez, L.F. (2002). Application of dilatometric analysis to the study of solid–solid phase transformations in steels. *Materials Characterization*. 48(1), 101-111. DOI: 10.1016/S1044-5803(02)00259-0.
[23] Jimbert, P., Guraya, T., Kaltzakorta, I., Gutierrez, T., Elvira, R. & Khajavi, L.T. (2022). Different phenomena encountered during dilatometryof low-density steels. *Journal of Materials Engineering and Performance*. 31(4), 2878-2888. DOI: 10.1007/s11665-021-06418-4.
[24] Wang, X., Zurob, H., Xu, G., Ye, Q., Bouaziz, O. & Embury. D. (2012). Influence of microstructural length scale on the strength and annealing behaviour of pearlite, bainite, and martensite. *Metallurgical and Materials Transactions A*. 44(3), 1454-1461. DOI: 10.1007/s11661-012-1501-1.
[25] Marques, M.C.S., de Moura, A.N., de Alcantara, C.M., de Carvalho, F.M.S.B., Bussoloti, R., Labiapari, W.S. & Vatavuk, J. (2023). Microstructure and mechanical properties of a martensitic stainless steel (0.2%C–12%Cr) after quenching and partitioning (Q&P) process. *Journal of Materials Research and Technology*. 24, 3937-3955. DOI: 10.1016/j.jmrt.2023.04.018.
[26] Sakuma, Y., Matsumura, O. & Takechi, H. (1991). Mechanical properties and retained austenite in intercritically heat-treated bainite-transformed steel and their variation with Si and Mn Additions. *Metallurgical Transactions A*. 22, 489-498. DOI: 10.1007/BF02656816.
[27] Balogun, D., Roman, M., Rex E. Gerald II, L. Bartlett, L., Huang, J. & O'Malley, R. (2023). A study on the impact of silicon and manganese on peritectic behaviour in low alloy steels assisted by mold thermal mapping technology and shell growth measurements. *Metallurgical and Materials Transactions B*. 54(3), 1326-1341. DOI: 10.1007/s11663-023-02764-x.
[28] Caballero, F.G., Miller, M.K., Garcia-Mateo, C., Capdevila, C. & Garcia de Andres, C. (2008). Phase transformation theory: A powerful tool for the design of advanced steels. *The Journal of The Minerals, Metals & Materials Society*. 60(12), 16-21. DOI: 10.1007/s11837-008-0159-z.
[29] Toole, J.K., Benz, J., Vieira, I., Clark, A.J., Thompson, S.W. & Findley, K.O. (2020). Strengthening mechanisms influenced by silicon content in high temperature tempered martensite and bainite. *Materials Science and Engineering: A*. 786,139419. DOI: 10.1016/j.msea.2020.139419.
[30] Kim, B., Boucard, E., Sourmail, T., San Martin, D., Gey, N. & Rivera-Diaz-del-Castillo, P.E.J. (2014). The influence of silicon in tempered martensite: Understanding the microstructure–properties relationship in 0.5–0.6 wt.% C steels. *Acta Materialia*. 68, 169-178. DOI: 10.1016/j.actamat.2014.01.039.
[31] Morito, S., Tanaka, H., Konishi, R., Furuhara, T. & Maki, T. (2003). The morphology and crystallography of lath martensite in Fe-C alloys. *Acta Materialia*. 51(6), 1789-1799. DOI: 10.1016/S1359-6454(02)00577-3.
[32] Kinney, C.C., Pytlewski, K.R., Khachaturyan, A.G. & Morris Jr. J.W. (2014). The microstructure of lath martensite in quenched 9Ni steel. *Acta Materialia*. 69, 372-385. DOI: 10.1016/j.actamat.2014.01.058.
[33] Stormvinter, A., Miyamoto, G., Furuhara, T., Hedstrom, P. & Borgenstam. A. (2012). Effect of carbon content on variant

pairing of martensite in Fe–C alloys. *Acta Materialia*. 60(20), 7265-7274. DOI: 10.1016/j.actamat.2012.09.046.
[34] Spanos, G. (1994). The fine structure and formation mechanism of lower bainite. *Metallurgical and Materials Transactions A*. 25(9), 1967-1980. DOI: 10.1007/BF02649045.
[35] Caballero, F.G., Miller, M.K. & Garcia-Mateo, C. (2014). Influence of transformation temperature on carbide precipitation sequence during lower bainite formation. *Materials Chemistry and Physics*. 146(1-2), 50-57. DOI: 10.1016/j.matchemphys.2014.02.041.
[36] Azuma, M., Fujita, N., Takahashi, M., Senuma, T., Quidort, D. & Lung, T. (2005). Modelling upper and lower bainite transformation in steels. *ISIJ International*. 45(2), 221-228. DOI: 10.2355/isijinternational.45.221.
[37] Furuhara, T., Kawata, H., Morito, S. & Maki, T. (2006). Crystallography of upper bainite in Fe–Ni–C alloys. *Materials Science and Engineering: A*. 431(1-2), 228-236. DOI: 10.1016/j.msea.2006.06.032.
[38] Yu, X., Wang, Y., Wu, H. & Gong. N. (2024). Ultra-fine bainite in medium-carbon high-silicon bainitic steel. *Materials*. 17(10), 2225, 1-16. DOI: 10.3390/ma17102225.
[39] Franceschi, M., Bettanini, A.M., Pezzato, L., Dabala, M. & Jacques, P.J. (2021). Effect of multi-step austempering treatment on the microstructure and mechanical properties of a high silicon carbide-free bainitic steel with bimodal bainite distribution. *Metals*. 11(12), 2055, 1-17. DOI: 10.3390/met11122055.
[40] Zhu, J., Sun, X., Barber, G., Han, X. & Qin, H. (2019). Effect of carbon content on bainite transformation kinetics and microstructure of 4140/4150 steels. *European Scientific Journal*. 15(9), 518-535. DOI: 10.19044/esj.2019.v15n9p518.